Programming Nanopore Ion Flow for Encoded Multiplex MicroRNA Detection

Xinyue Zhang[1], Yong Wang[1], Brandon L. Fricke[1], Li-Qun Gu[1*]

Supplementary Information

Table S1. Sequences of target miRNAs and their unlabeled and PEG-labeled DNA probes

miRNAs and Probes	Sequences (5'-3')
miR-155	rUrUrArArUrGrCrUrArArUrCrGrUrGrArUrArGrGrGrU
miR-155-probe-C30	ACCCCTATCACGATTAGCATTAACCCCCCCCCCCCCCCCCCCCCCCCCCCCCCCC
miR-155-probe-C30-alkyne2	ACCCCTATCACGATTAGCATTAACC/i5OctdU/CCCCCCCCCCCCCCCCCCCCCCCCCCCCCC
miR-182-5p	rUrUrUrGrGrCrArArUrGrGrUrArGrArArCrUrCrArCrArCrU
miR-182-5p-probe-C30	AGTGTGAGTTCTACCATTGCCAAACCCCCCCCCCCCCCCCCCCCCCCCCCCCCCC
miR-182-5p-probe-C30-alkyne2	AGTGTGAGTTCTACCATTGCCAAACC/i5OctdU/CCCCCCCCCCCCCCCCCCCCCCCCCCCCCC
miR-210	rCrUrGrUrGrCrGrUrGrUrGrArCrArGrCrGrGrCrUrGrA
miR-210-probe-C30	TCAGCCGCTGTCACACGCACAGCCCCCCCCCCCCCCCCCCCCCCCCCCCCCCCC
miR-210-probe-C30-alkyne2	TCAGCCGCTGTCACACGCACAGCC/i5OctdU/CCCCCCCCCCCCCCCCCCCCCCCCCCCCCC
miR-21	rUrArGrCrUrUrArUrCrArGrArCrUrGrArUrGrUrUrGrA
miR-21-probe-C30	TCAACATCAGTCTGATAAGCTACCCCCCCCCCCCCCCCCCCCCCCCCCCCCCCC
miR-21-probe-C30-alkyne2	TCAACATCAGTCTGATAAGCTACC/i5OctdU/CCCCCCCCCCCCCCCCCCCCCCCCCCCCCC

*/i5OctdU/: 5-octadiynyl deoxyuridine

Table S2. Ionic currents for the empty αHL pore (I_0) and various miRNA•probe signature (I), and their blocking levels (I/I_0) [a]

PEG tag[b]		miR-155	miR-21	miR-210	miR-182-5p
	I_0 (pA)	121.02±0.03	117.08±1.04	119.65±0.34	121.49±0.03
No tag	I (pA) [c]	14.56±0.11	11.71±1.07	12.60±0.05	13.94±0.04
	I/I_0	**(12.0±0.1)%**[d]	(10.0±1.8)%	(10.5±0.3)%	(11.5±0.1)%
	I_0 (pA)	121.99±0.03	120.10±0.35	124.76±0.23	125.46±0.28
PEG3	I (pA)	9.23±0.03	8.28±0.46	9.51±0.04	11.43±0.03
	I/I_0	(7.6±0.1)%	(6.9±0.7)%	(7.6±0.2)%	**(9.1±0.3)%**
	I_0 (pA)	126.86±0.32	122.99±0.22	131.12±0.49	122.59±0.30
PEG8	I (pA)	7.60±0.03	7.46±1.35	7.27±0.03	8.26±0.03
	I/I_o	(6.0±0.3)%	(6.1±1.3)%	**(5.6±0.4)%**	(6.7±0.3)%
	I_0 (pA)	122.63±0.03	130.16±0.08	124.70±0.33	118.18±0.40
PEG24	I (pA)	2.34±0.04	1.92±0.15	2.51±0.03	2.89±0.03
	I/I_0	(1.9±0.1)%	**(1.5±0.2)%**	(2.0±0.3)%	(2.4±0.4)%

[a]: Recorded in 1 M KCl, 10 mM Tris (pH 7.4) at +120 mV.

[b:] Types of PEG tag on the probe. The probe sequence is shown in Table S1.

[c]: Currents of stage I in signatures with untagged probe (P0) or stage Ib in signatures with PEG-tagged probes (P3, P8 and P24). Both signatures are dissected in Fig. 2.

[d]: Bolded I/I_0 values are for four miRNAs hybridized by a set of optimal barcode probes with maximally separated blocking levels.

S1. miRNA sequence-dependent signature duration

The barcoded miRNA•probe signatures are not only characterized by distinct blocking levels, but also their duration are dramatically different to each other (Fig. 3). It has been understood in the main text that the blocking level is modulated by the PEG tag. Here we demonstrate that the signature duration is independent of the PEG tag, but is mainly regulated by the miRNA sequence.

Determining signature duration. The scatter plots in Fig. S3 shows the distribution of the blocking level (I/I_0) and duration (t) for recorded events. The framed events with the characteristic blocking level are miRNA•probe signatures. For example, the framed events centered at I/I_0=12% in Fig. S3a are miR-155 signatures with an untagged probe, and that around I/I_0=5.6% in Fig. S3b are miR-210 signatures with a PEG8-tagged probe. In addition, there are events at higher block levels and with shorter duration. They may be formed by the hybrids that interact with the pore differently. For example, the hybrid may be trapped in the nanocavity, but not in the β-barrel; or it may enter the pore in the opposite direction with the duplex domain first trapped in the pore.[1] Fig. S4 show the event duration histograms for all types of tagged (panel a-d) and untagged (panel e-h) probes. According to the scatter plots such as that shown in Fig. S3, the long component in each histogram is the miRNA•probe signatures. The duration constant can be obtained by fitting this component to a log probability exponential distribution. The shorter components in these histograms are not signatures, and cannot participate in the analysis of signature duration.

PEG tag, miRNA sequence and signature duration. Fig. 3c show the signature duration for different miRNAs using both untagged probes (black bar) and PEG-tagged

probes (barcode probes, grey bar). Clearly the signatures for miR-182-5p•P3 (11±2s) and miR-210•P8 (9.3±2.1s) hybrids are over 100 times prolonged compared with miR-155•P0 (33±4ms) and miR-21•P24 (44±2ms) hybrids (grey bar). When the four untagged probes are used in place of tagged-probes, the miRNA•probe signature duration shows exactly the same trend as that using tagged-probes (black bar), suggesting that the PEG tag does not influence the signature duration. On the other hand, we have understood that the unzipping of the miRNA•probe hybrid in the pore dominates the entire signature duration (Stage I in Fig. 2). We therefore compared the factors such as melting temperature (T_m) that may influence the unzipping process. Fig. 3c shows that T_m for miR-182-5p and miR-210 are indeed significantly higher than miR-155 and miR-21 due to their higher GC content. By comparison, the large variation in signature duration among the four miRNAs is qualitatively consistent with their melting temperatures (T_m) difference. This means the miRNA sequence is an important factor to regulate the unzipping time, and thus the signature duration. Sequences giving higher T_m can hybridize with their probes more strongly, leading to a prolonged unzipping procedure in the nanopore.

S2. Optimum barcode motif and tagging position

Sensitive multiplex detection relies on accurate discrimination of signature blocking levels. Here we demonstrate the influence of barcode motifs and labeling positions on the signature blocking level.

Barcode motifs. We tested polyethylene glycol (PEG) as a representative polymer compound, and TET (popular fluorescein dye for labeling oligonucleotides) as a representative non-polymer compound. Both compounds have commercially available derivatives for "click" conjugation with oligonucleotides. They were linked to 5-octadiynyl deoxyuridine between C2/C3 on the poly$(dC)_{30}$ lead of the probe (Table S1 for the probe sequences). Each tagged probe was hybridized with the target miRNA. The miRNA•probe signature using TET- tagged probe are shown in Fig. S5, and that using PEG-tagged probe has been dissected in Fig. 2. The signatures indicate that both compounds can exclude the volume in the nanopore ion pathway and block the pore current. Fig. S5 shows that the TET tag generates permanent blockade, which can only be resumed by applying a negative voltage. Also the background current of the blocking level is highly noisy, making it difficult to dissect the configuration change of the hybrid in the pore. In contrast, Fig. 2 has shown that the PEG tag clearly reveals multiple distinct stages for trapping, unzipping and translocation of the complex in the nanopore. Different from TET, the PEG volume exclusion can be simply programmed with the polymer length. This property allows each PEG species to produce a specific blocking level, therefore is favorable for barcode design. In addition, PEG is soluble, flexible and is unlikely to fold with the target nucleic acids to affect its structure. Compared with other polymers such as polypeptides, the conjugation with PEG is cost-efficient. Overall, a set

of PEGs with designated lengths can be used as an optimal barcode motif for multiplex detection.

Tagging position. The barcode position on the probe also influences the signature blocking level. Fig. S6 compares two signatures for different PEG8 tagging positions. The target is miR-210. When the miR-210•probe hybrid is pulled into the nanopore, the poly(dC)$_{30}$ lead of the probe is first trapped in the β-barrel. Fig. S6a shows the signature with PEG8 tagged to 5-octadiynyl deoxyuridine between C2/C3 on the poly(dC)$_{30}$ lead. This position is located within the constrictive region of the pore (1.5 nm wide). The ionic current is very sensitive to the molecule occupying this region. Fig. 2 has shown that the PEG tag splits the unzipping stage I of the signature into Ia, Ib, and Ic. Among the three domains, Ia and Ic represent the configuration in which PEG is not presented in this sensing zone, and Ib represents a configuration in which PEG occupies this region during unzipping. This configuration change generates a 5.7 pA current difference between stages Ib and Ia (or Ic) (+120 mV). This current change is sufficiently big to be accurately distinguished by the amplifier with a resolution at 0.1 pA. In contrast, Fig. S6b shows the signature with PEG8 tagged at C5/C6 on the same probe. In this signature, the entire stage I for unzipping becomes flat, and there is no distinct stage Ia, Ib and Ic. Given that the inter-base distance in a single-stranded DNA is 0.7 nm,[2] this position should be approximately 4.2 nm away from the double-stranded domain. Because the entire β-barrel is 5-nm long, this tagging position should be close to the trans opening. Therefore this finding suggests that there is no significant current difference between PEG8 occupying and not occupying the region around the pore trans opening. In other words, the blocking level is not sensitive to the PEG8 located in this region. Overall, the

PEG tagging position influences the amplitude of the signature blocking level. The position C2/C3 is a favorable sensing zone for PEG barcode construction.

S3. Several issues in multi-target quantification

Signature frequency analysis in multiplex miRNA detection. In multiplex miRNA detection, different miRNA signatures are recorded simultaneously in a current trace. The occurring frequency of each signature can be measured to quantify each the miRNA in the mixture. The signature frequency for miRNA i, f_i, can be determined in 4 steps:

1) Determine the average inter-event interval, τ_{on}. This is duration between two adjacent signatures, from the end of one signature to the beginning of the next signature.

2) Determine the total signature frequency $f=1/\tau_{on}$. This is the sum of frequencies of all types of miRNA•probe signatures, $f=\Sigma f_i$.

3) Calculate the fraction of each type of signature. In an event amplitude histogram, the area under each peak is the number of that type of signature, N_i. Its fraction in the total signatures is $N_i/\Sigma N_i$.

4) Calculate the frequency of a type of signature from the total frequency and the fraction, $f\cdot(N_i/\Sigma N_i)$.

Event number *versus* detection error in duration measurement. In nanopore single-molecule detection, both individual event duration and inter-event duration are stochastic, and follow the exponential distribution. Analysis with lower number of events may cause a larger variation (inaccuracy). Here we investigate the correlation between the number of events collected *versus* the relative error in duration measurement. This relationship allows for evaluating how many events are sufficient to meet a designated error level. This investigation has been conducted through simulation as follow,

1) Generate n columns (n=4) of exponentially distributed stochastic duration values using the same constant τ to simulate n independent measurements. Each column contains m events (m=200).

2) In each column i (i=1 to n), randomly select j events (j=1, 2, …, m) to form a subgroup. There are total m subgroups. Calculate the mean duration of each subgroup τ_{ij}.

3) For all n subgroups that contains j events, calculate the mean of all τ_{ij} from n columns, $\tau_j = (\sum_{i=1}^{n} \tau_{ij})/n$ and corresponding standard deviation σ_j. Then calculate the relative error σ_j/τ_j for all the subgroups containing j events.

4) Repeat step 1 to 3 for l times (l=20), and calculate their mean relative error $(\Sigma\sigma_j/\tau_j)/l$ for each j.

5) Plot the mean relative error versus the number of events j.

Fig. S7 shows the plot for event number-dependent relative error based on the simulation result. According to this correlation, the relative error rapidly decays as the event number increases. Measurement with 20 exponentially distributed events would have a relative error of 20%, and 70 events would be sufficient to achieve a relative error of 10% (marked by two red circles in Fig. S7). To further reduce the relative error to 5%, the measurement needs to involve 200 events. This correlation is applicable to both event duration and inter-event duration (for calculating the frequency), which are both exponentially-distributed.

Detection limits. In single-molecule sensing, the target concentration can be read out from the occurring frequency of signature. Because single-molecule events are stochastic, a sufficient number of signature blocks needs to be analyzed to ensure the

result is within a relative error. As low target concentration results in low event frequency, to collect sufficient number of events, the recording time should be prolonged. Therefore, to determine the minimal target concentration that can be detected or detection limit, we need to 1) set an error level, 2) evaluate the minimal number of events to reach that error level, and 3) set a limit of recording time. We have utilized a large set of simulated single-molecule data to obtain the event number-dependent duration relative error (Fig. S8). According to this correlation, analysis with 70 events would be sufficient to reach the 10% relative error, and 100 events would secure this result. Our current setup allows sustaining the lipid bilayer for a couple of hours. If setting 2 hours as the maximal recording time, then the minimal frequency available for 70 events in 2 hours in one nanopore would be 0.01 s^{-1}. Through this method, the miRNA concentration at 10 pM was determined (Fig. 4d). In practice, multiple nanopores can be used to analyze target at low concentration. Due to multi-fold increase in the event number as the multiple nanopores participate in recording, the actual frequency would be the recorded frequency divided by the number of pores[3]. For five channels, the detection limit can be improved to 1-2 pM.

Other methods can be integrated to enhance the detection limit, for example 1) recording in asymmetric solution,[4] 2) constructing charged amino acids lining the ion pathway of the pore to enhance the trapping of oligonucleotide into the nanopore,[5] 3) recording in miniaturized chamber such as droplet interface bilayer[6] to avoid intensive dilution of the sample. Recently we have shown that the use functionally engineered probe can selectively detection the target nucleic acids in a mixture with high sensitivity.[7]

Influence of event duration on sensor performance. The total recording time

for a nanopore current trace consists of two parts, total blocking time (sum of all the block duration) and total unblocking time (sum of all the inter-block duration). The inter-event duration is measured as the time from the end of one block to the beginning of the next block. For long blocks, the total blocking time should be long. This needs to extend the total recording time in order to collect sufficient number of events for accurate measurement. However, we expect that this time extension has NO significant influence on the overall detection efficiency. For example, if we need to record 200 blocks with duration of 5 sec, their total blocking time should be 5×200=1000 sec or 17 min. If these blocks occur at a frequency of 0.1 s^{-1}, the total unblocking time will be (1/0.1)×200=2000 sec or 34 min. This means we need to extend the recording time by 17 min from 34 min to 51 min to collect these blocking events. This 17 min is not a significant extension compared with our normal 1-2 hours recording time. This means that, although collecting sufficient number of long blocks requires extended recording time, this time extension has no significant influence on the sensing performance. The extended recording time is still much shorter compared with other approaches such as qRT-PCR, which takes at least a couple of hours for the entire procedure (our experience). In fact, long event duration also has merits. It makes the miRNA•probe signature more distinguishable from others, therefore enhancing the multiplex detection specificity.

S4. Comparison of the nanopore with current approaches

Disease diagnostics requires rapid and accurate detection of miRNA biomarkers in tissues and biofluids. Common commercial technologies for miRNA detection include, but not limit to qRT-PCR,[8] microarrays,[9] next-generation sequencing[10] and the newcomer NanoString.[11] There are also many emerging methods such as in situ hybridization[12] (not quantitative), nanoparticle,[13] barcode,[14] deep sequencing[15] and single-molecule fluorescence.[16]

Northern blotting was a powerful approach in early time to identify new miRNAs. This approach is laborious and needs a large amount of samples (microgram scale). Microarray was then adapted for miRNA profiling. The most important merit of microarray is high throughput, but the detection is semi-quantitative and miRNAs need fluorescence-labeling. Its popularization was hindered by its multistep procedures and the usage of large amount samples.

At present, quantitative reverse transcript PCR (qRT-PCR) is the gold standard for miRNA detection in tissue or plasma extract. The amplification procedure makes this approach extremely sensitive, with a very low detection limit at 10 fM level. PCR also allows multiplex detection. On the other hand, target RNAs have to be transformed into DNA (reverse transcription) for amplification. The small length of miRNAs (18-24 nts) makes it difficult to design two opposite primers, and requires for chemical extension of miRNA sequences. All these steps, miRNA extension, cDNA generation and DNA amplification, need chemical modification or enzymatic reaction, making the entire procedure complicated, expensive and time-cost. Although the PCR itself is sensitive, the result often has a large variation due to multi-steps involved, and the entire course may

take at least a couple of hours to one day. PCR is also highly sensitive to the contamination with genomic DNA, which may generate more false positive results.

Recently, the Next Generation Sequencing provides a powerful platform for discovering new miRNAs. The sequencing approaches also require ligation of a DNA linker to the miRNA, followed by PCR amplification. NGS has greatly expanded the power for the discovering new miRNAs, but it is semi-quantitative. It is normally used for genomewide screening, and its role in clinical diagnostics is limited by high cost.

The nanopore performs direct miRNA detection at single-molecule level. It does not need covalent labeling or enzymatic treatment for the target miRNAs. This "mix-then-count" detection is relatively simpler, cheaper and more time-efficient. The target concentration can be obtained in proportion to the signature frequency with lower variation.[17] Optimized system can detect 100 fM miRNAs.[17] This level is sufficient for miRNA detection in biofluids, whose concentration highly depends on the miRNA species, tissue types and efficiency in total RNA extraction and enrichment. One advantage of single-molecule detection is that the single-molecule signature allows target discrimination with high specificity in the presence of a large number of non-target sequences or contaminants. The nanopore has also been demonstrated to discriminate different targets with similar sequences.[7, 17]

The nanopores also face challenges in translating this approach into a clinically usable tool. As studied in this report, multiplex miRNA detection is important for rapid disease diagnostics. This capability is demanded in competing with other high throughput techniques. In this report, the study of biophysical mechanism for programming ionic flow is an important step toward this goal, though there is still a long validation study in

clinical samples. In addition to this challenge, we have recently invented a molecular approach that allow selectively driving of the target miRNA into the pore[7] for highly specific and sensitive detection in complex nucleic acids mixture. Moreover, the use of miniaturized system such as droplet-interfaced bilayer can greatly reduce the sample amount to great improve the detection limit.[6] Overall, the nanopore is a potential tool for accurate analysis of nucleic acids including miRNAs for both research and diagnosis. Recently Oxford Nanopore Inc launched the first nanopore chip for rapid sequencing.

References:

1. Japrung, D.; Henricus, M.; Li, Q.; Maglia, G.; Bayley, H., Urea Facilitates the Translocation of Single-Stranded DNA and RNA through the Alpha-Hemolysin Nanopore. *Biophys. J.* **2010,** *98*, 1856-63.
2. Murphy, M. C.; Rasnik, I.; Cheng, W.; Lohman, T. M.; Ha, T., Probing Single-Stranded DNA Conformational Flexibility Using Fluorescence Spectroscopy. *Biophys. J.* **2004,** *86*, 2530-2537.
3. Ervin, E. N.; White, R. J.; White, H. S., Sensitivity and Signal Complexity as a Function of the Number of Ion Channels in a Stochastic Sensor. *Anal. Chem.* **2009,** *81*, 533-7.
4. Wanunu, M.; Morrison, W.; Rabin, Y.; Grosberg, A. Y.; Meller, A., Electrostatic Focusing of Unlabelled DNA into Nanoscale Pores Using a Salt Gradient. *Nat. Nanotechnol.* **2010,** *5*, 160-165.
5. Maglia, G.; Restrepo, M. R.; Mikhailova, E.; Bayley, H., Enhanced Translocation of Single DNA Molecules Through α-Hemolysin Nanopores by Manipulation of Internal Charge. *Proc. Natl. Acad. Sci. U. S. A.* **2008,** *105*, 19720-19725.
6. Bayley, H.; Cronin, B.; Heron, A.; Holden, M. A.; Hwang, W. L.; Syeda, R.; Thompson, J.; Wallace, M., Droplet Interface Bilayers. *Molecular BioSystems* **2008,** *4*, 1191-1208; Fischer, A.; Holden, M. A.; Pentelute, B. L.; Collier, R. J., Ultrasensitive Detection of Protein Translocated through Toxin Pores in Droplet-Interface Bilayers. *Proc. Natl. Acad. Sci. U. S. A.* **2011,** *108*, 16577-81.
7. Tian, K.; He, Z.; Wang, Y.; Chen, S. J.; Gu, L. Q., Designing a Polycationic Probe for Simultaneous Enrichment and Detection of MicroRNAs in a Nanopore. *ACS Nano* **2013,** *7*, 3962-3969.
8. Hunt, E. A.; Goulding, A. M.; Deo, S. K., Direct Detection and Quantification of MicroRNAs. *Analytical Biochemistry* **2009,** *387*, 1-12; Murphy, J.; Bustin, S. A., Reliability of Real-Time Reverse-Transcription PCR in Clinical Diagnostics: Gold Standard or Substandard? *Expert Rev. Mol. Diagn.* **2009,** *9*, 187-197.
9. Lu, J.; Getz, G.; Miska, E. A.; Alvarez-Saavedra, E.; Lamb, J.; Peck, D.; Sweet-Cordero, A.; Ebert, B. L.; Mak, R. H.; Ferrando, A. A.; *et al*., MicroRNA Expression Profiles Classify Human Cancers. *Nature* **2005,** *435*, 834-838.
10. Su, Z.; Ning, B.; Fang, H.; Hong, H.; Perkins, R.; Tong, W.; Shi, L., Next-Generation Sequencing and Its Applications in Molecular Diagnostics. *Expert Rev. Mol. Diagn.* **2011,** *11*, 333-343.
11. Raison, C., Preterm Birth Risk Diagnostic Test to Be Given Boost by Partnership between Agilent Technologies and Sera Prognostics. *Expert Rev. Mol. Diagn.* **2013,** *13*, 230.
12. Kloosterman, W. P.; Wienholds, E.; de Bruijn, E.; Kauppinen, S.; Plasterk, R. H., *In Situ* Detection of MiRNAs in Animal Embryos Using LNA-Modified Oligonucleotide Probes. *Nat. Methods* **2006,** *3*, 27-29.
13. Alhasan, A. H.; Kim, D. Y.; Daniel, W. L.; Watson, E.; Meeks, J. J.; Thaxton, C. S.; Mirkin, C. A., Scanometric MicroRNA Array Profiling of Prostate Cancer Markers Using Spherical Nucleic Acid-Gold Nanoparticle Conjugates. *Anal. Chem.* **2012,** *84*, 4153-4160; Raison, C., Gold Nanoparticle-Based Diagnostic Test for Rapid Diagnosis of Leading Infectious Diseases. *Expert Rev. Mol. Diagn.* **2013,** *13*, 230.

14. Chapin, S. C.; Appleyard, D. C.; Pregibon, D. C.; Doyle, P. S., Rapid MicroRNA Profiling on Encoded Gel Microparticles. *Angew. Chem. Int. Ed.* **2011,** *50*, 2289-2293.
15. Yendamuri, S.; Kratzke, R., MicroRNA Biomarkers in Lung Cancer: MiRacle or quagMiRe? *Transl. Res.* **2011,** *157*, 209-215.
16. Neely, L. A.; Patel, S.; Garver, J.; Gallo, M.; Hackett, M.; McLaughlin, S.; Nadel, M.; Harris, J.; Gullans, S.; Rooke, J., A Single-Molecule Method for the Quantitation of MicroRNA Gene Expression. *Nat. Methods* **2006,** *3*, 41-46.
17. Wang, Y.; Zheng, D.; Tan, Q.; Wang, M. X.; Gu, L. Q., Nanopore-Based Detection of Circulating MicroRNAs in Lung Cancer Patients. *Nat. Nanotechnol.* **2011,** *6*, 668-674.

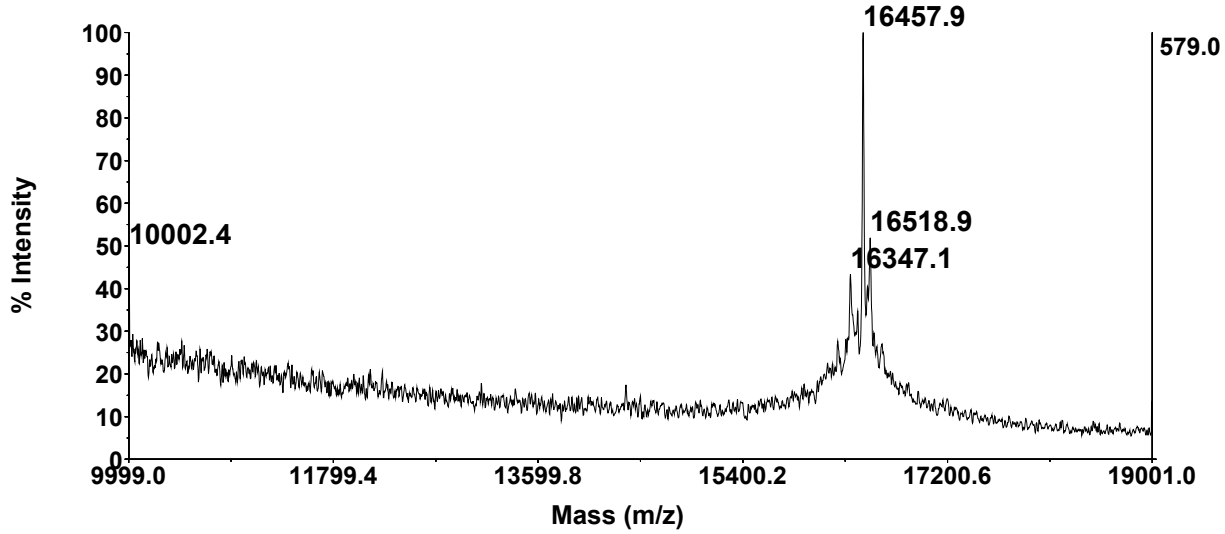

Figure S1. MALDI-TOF mass spectrogram of PEG8-labeled DNA probe for miR-155. As exemplified by miR-155-probe-C30-alkyne2-PEG8, the calculated m/z value of the product was 16458.9 and the measured value was 16457.9.

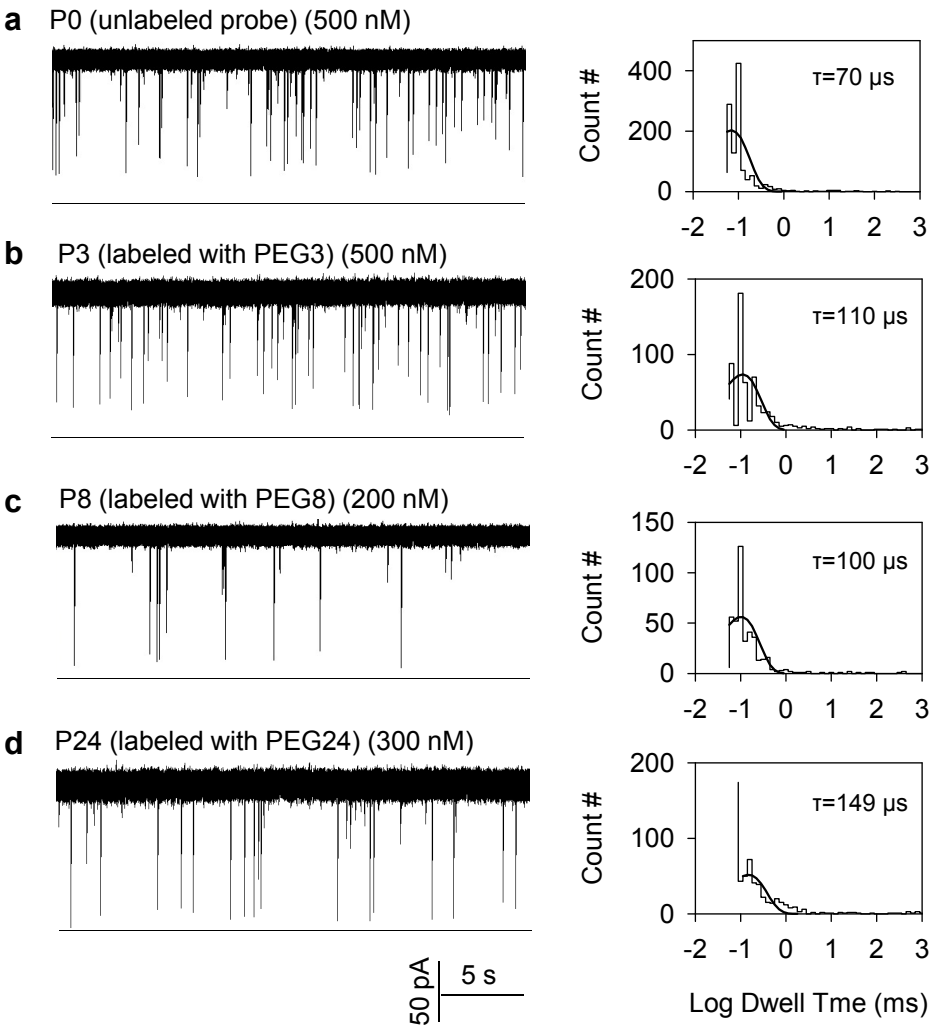

Figure S2. Current traces and block duration histograms for translocation of untagged and PEG-tagged probes through the αHL pore. **a,** Untagged miR-155 probe. **b-d,** PEG3- (b), PEG8- (c) and PEG24- (d) tagged miR-155 probes. PEGs were conjugated to 5-octadiynyl deoxyuridine between C2/C3 on the poly$(dC)_{30}$ lead. Currents were recorded at +120 mV in 1 M KCl buffered with 10 mM Tris (pH7.4). Histograms were fitted to the exponential distribution (log probability) to obtain the time constant. Translocation duration for all the probes alone was in the 10-100 μs sale, and completely distinguished from the miRNA•probe signatures that last from tens of milliseconds to several seconds (S4 and Fig. S4).

S2. miRNA sequence-dependent signature duration

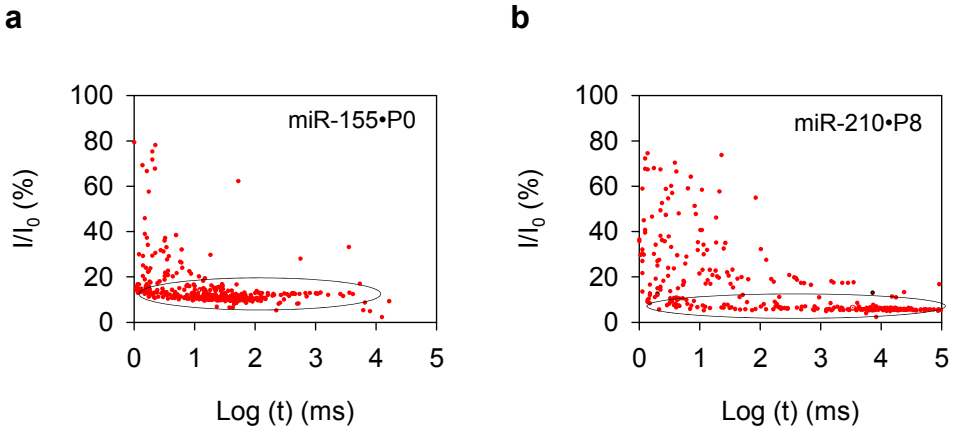

Figure S3. Scatter plots showing the distribution of block duration and blocking levels for different miRNA•probe complexes. The blocking level is measured as I/I_0 (%), where I_0 is the current through an open pore and I is the current of the block. **a,** miR-155 in complex with an untagged probe. **b,** miR-210 in complex with a PEG8-tagged probe. Data was obtained from current traces recorded at +120 mV in 1 M KCl buffered with 10 mM Tris (pH7.4). The majority of points that were covered by ellipses featured the signature current levels, which were I/I_0=12% for untagged probe (a) and I/I_0=5.6% for PEG8-tagged probe. They corresponded to the long component in the event duration histogram (Fig. S4).

S2. miRNA sequence-dependent signature duration

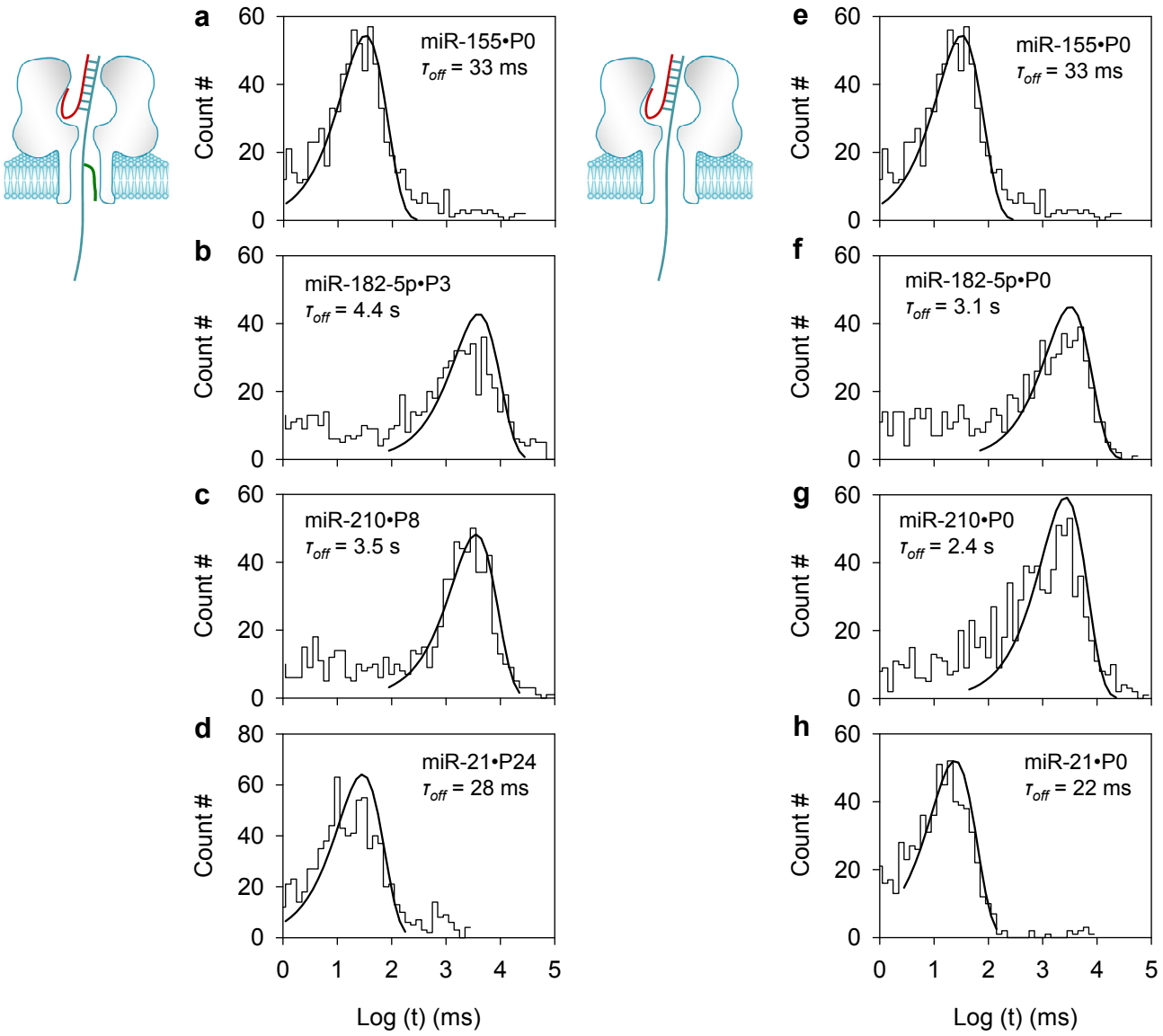

Figure S4. Event duration histograms for calculating the miRNA•probe signature duration. **a-d**, for miRNAs hybridized with barcode probes: miR-155 with P0 (untagged, a), miR-182-5p with P3 (PEG3 tag, b), miR-210 with P8 (PEG8 tag, c), and miR-21 with P24 (PEG24 tag, d). **e-h**, for miRNAs hybridized with untagged probes: miR-155 (e), miR-182-5p (f), miR-210 (g), miR-21 (h). The long component in each histogram was the miRNA•probe signatures (see scatter plots in Fig. S3), and was fitted to a log probability exponential distribution.

S3. Optimal barcode motif and tagging position

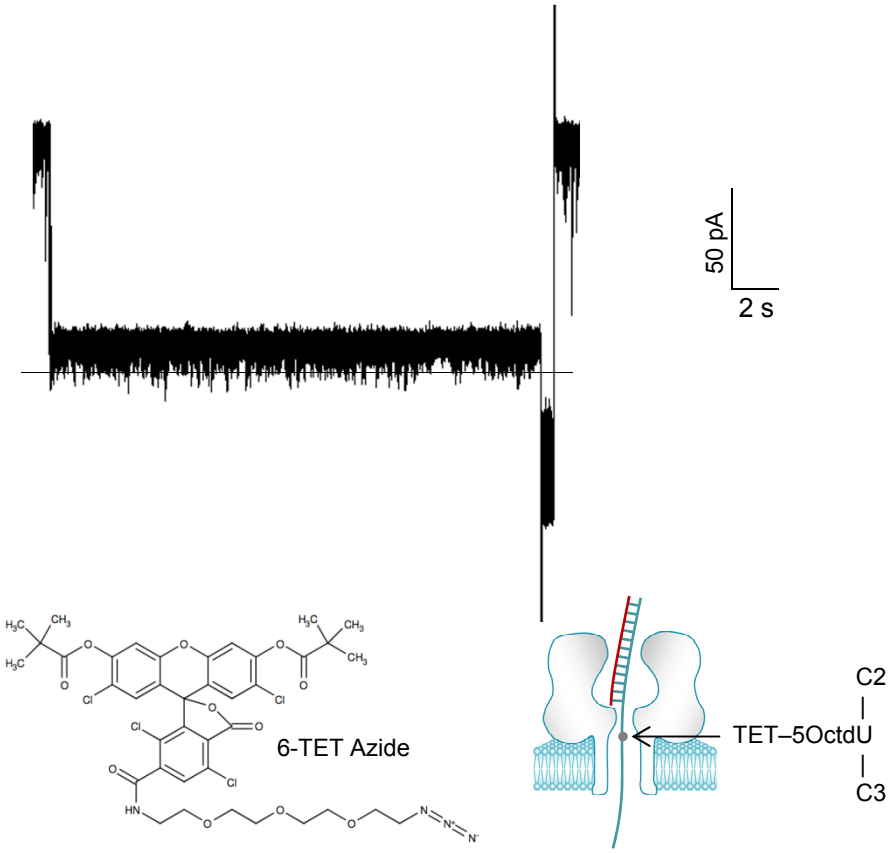

Figure S5. miRNA•probe block with TET tagged on the probe. The short strand (red) is miRNA (miR-155), and the long strand (aqua) is the probe, which was tagged with a TET to 5-octadiynyl deoxyuridine between C2/C3 of the lead. With TET tagged, the miRNA•probe hybrid permanently blocked the nanopore, and the blocking current is highly noisy.

S3. Optimal barcode motif and tagging position

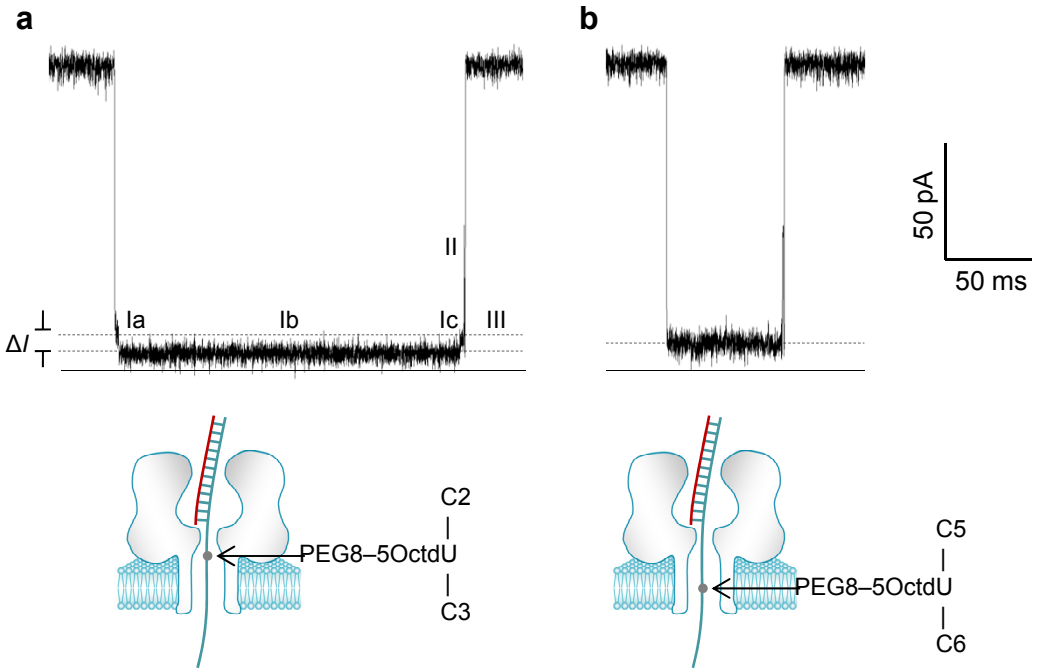

Figure S6. Barcode position-dependent signature blocking level. The probe for miR-210 was linked with a PEG8. The short strand (red) represents miRNA (miR-210), and the long strand (aqua) is the probe. PEG8 is tagged on the poly(dC)$_{30}$ lead of the probe. **a,** miRNA•probe signature with PEG8 linked to 5-octadiynyl deoxyuridine between C2/C3, a position within the constrictive region in the β-barrel when trapped in the pore. **b,** Signature for PEG8 tagged between C5/C6. Given that the entire β-barrel is 5-nm long and the inter-base distance in a ssDNA is 0.7 nm, this position should be approximately 4.2 nm away from the duplex domain. Upon trapped in the pore, this position is close to the trans opening. The current was recorded at +120 mV in 1 M KCl buffered with 10 mM Tris (pH7.4). The two signatures shows that PEG8 between C5/C6 (b) reduces less current and does not form distinct stages that reveal the unzipping procedure, compared with tagging at C2/C3 (a).

S4. Quantification of multiplex miRNAs

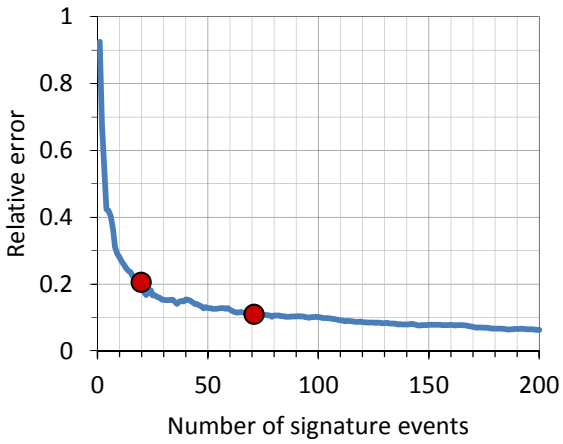

Figure S7. Correlation between the signature event number and the measuring relative error. This relationship is applicable to the analysis of signature duration and signature frequency, both of which follow the exponential distribution. Two red dots mark the number of signature events required for reaching the relative error levels at 10% and 20%.

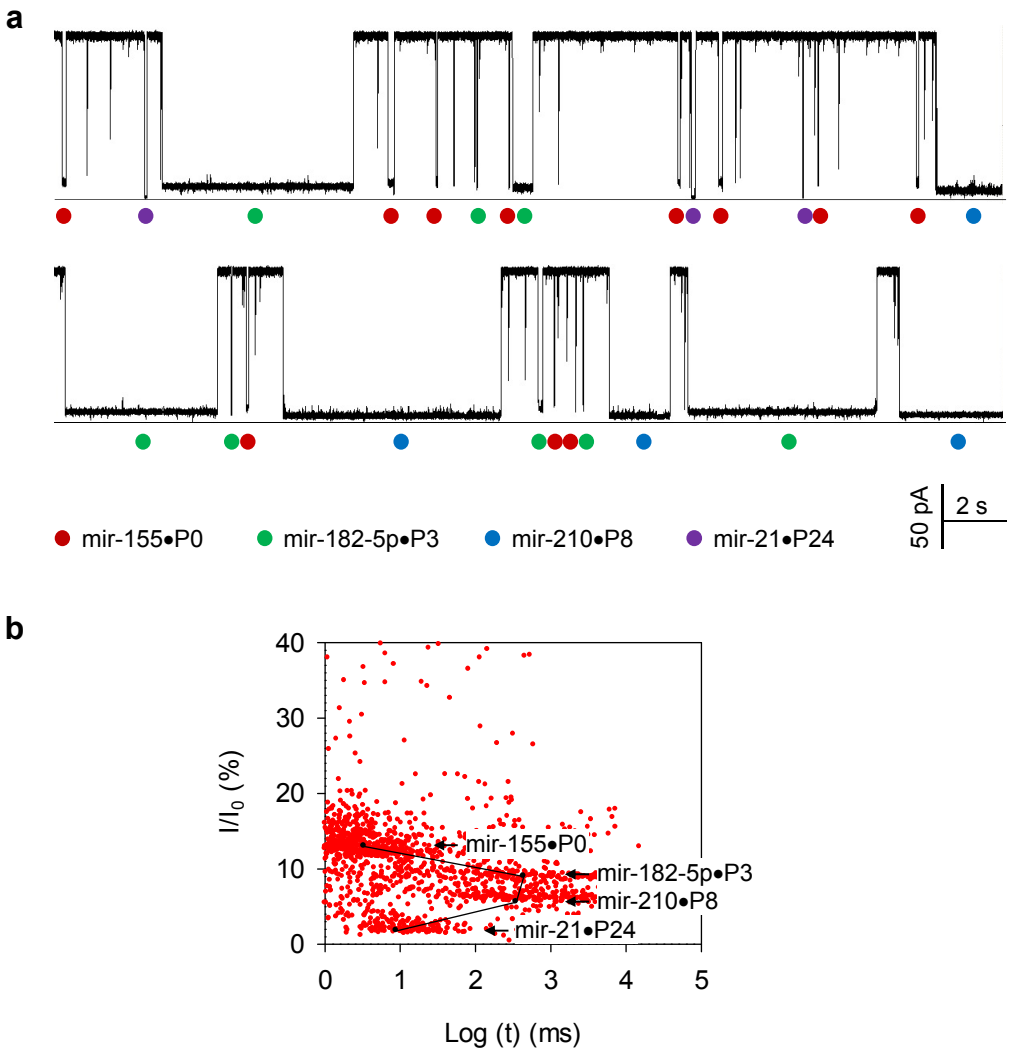

Figure S8. a, Simultaneously identification of various miRNA•probe signatures in a current trace. Each color dot marks one miRNA•probe signature. Four miRNA•probe signatures identified were marked in different colors and can be discriminated from specific blocking levels. The four target miRNAs were miR-155 (300 nM), miR-182-5p (75 nM), miR-210 (75 nM) and miR-21 (75 nM). Their probes, P0 (350 nM), P3 (100 nM), P8 (100 nM) and P24 (100 nM) were unlabeled, labeled with a PEG3, PEG8 and PEG24 respectively. Current trace was recorded at +120 mV in 1 M KCl buffered with 10 mM Tris (pH7.4); **b,** Blocking level (I/I_0) – block duration (t) scatter plot for the trace in Fig. 4a (main text), showing the separation of the multiple (four) miRNA•probe complexes based on both of their amplitudes and duration. The histogram of current amplitudes for these blocks is shown in Fig. 4b (main text). The fitted average event conductance and event duration are superimposed on the scatter plot (black dot and line).